J. Fluid Mech. (1989), *vol.* 207, *pp.* 311–321
Printed in Great Britain

Experimental investigation of convective stability in a superposed fluid and porous layer when heated from below

By FALIN CHEN† AND C. F. CHEN
Department of Aerospace and Mechanical Engineering, University of Arizona, Tucson, AZ 85721, USA

(Received 8 August 1987 and in revised form 15 March 1989)

Experiments have been carried out in a horizontal superposed fluid and porous layer contained in a test box 24 cm × 12 cm × 4 cm high. The porous layer consisted of 3 mm diameter glass beads, and the fluids used were water, 60% and 90% glycerin–water solutions, and 100% glycerin. The depth ratio $\hat{d}$, which is the ratio of the thickness of the fluid layer to that of the porous layer, varied from 0 to 1.0. Fluids of increasingly higher viscosity were used for cases with larger $\hat{d}$ in order to keep the temperature difference across the tank within reasonable limits. The top and bottom walls were kept at different constant temperatures. Onset of convection was detected by a change of slope in the heat flux curve. The size of the convection cells was inferred from temperature measurements made with embedded thermocouples and from temperature distributions at the top of the layer by use of liquid crystal film. The experimental results showed (i) a precipitous decrease in the critical Rayleigh number as the depth of the fluid layer was increased from zero, and (ii) an eightfold decrease in the critical wavelength between $\hat{d} = 0.1$ and 0.2. Both of these results were predicted by the linear stability theory reported earlier (Chen & Chen 1988).

1. Introduction

In an earlier publication (Chen & Chen 1988), we studied the onset of salt-finger convection in a superposed fluid and porous layer by linear stability theory. The motion in the fluid layer was governed by the Navier–Stokes equation, and the motion of the fluid in the porous layer was governed by the Darcy equation. Because of the differences in the order of the differential equations involved, a velocity slip condition proposed by Beavers & Joseph (1967) was applied at the interface. It was further assumed that the motion was two-dimensional and the layers were of infinite horizontal extent. In order to check the method of analysis and the associated computational program, we first calculated the onset of conditions for a pure thermal convection case and compared our results with those of Sun (1973).

For the thermal convection case at a given depth ratio $\hat{d}$ (the ratio of the fluid layer depth to porous layer depth), the critical conditions are determined by three other parameters: the Darcy number δ, the ratio of thermal diffusivities ϵ_T, and the accommodation coefficient $\hat{\alpha}$ at the interface. The Darcy number $\delta = K^{\frac{1}{2}} d_m^{-1}$, where K is the permeability and d_m the layer thickness of the porous medium. The thermal diffusivity ratio $\epsilon_T = \kappa_f/\kappa^*$, in which κ_f is the thermal diffusivity of the fluid and κ^* is the thermal diffusivity of the porous medium defined as the ratio of

† Present address: Institute of Applied Mechanics, National Taiwan University, Taipei, Taiwan 10764, ROC.

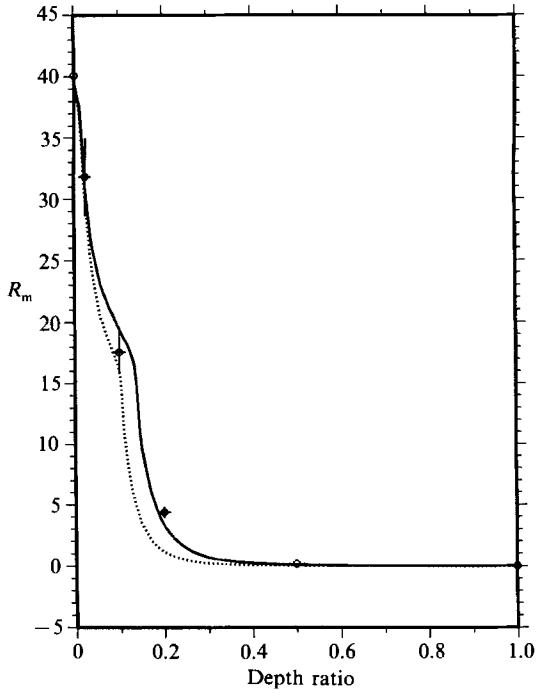

FIGURE 1. Variation of the critical Raleigh number with depth ratio. The solid line is for $\delta = 1.77 \times 10^{-3}$ and $\epsilon_T = 0.7$ appropriate for a water-saturated porous layer of 4 cm thickness; the dotted line is for $\delta = 3.53 \times 10^{-3}$ and $\epsilon_T = 0.4$ appropriate for a glycerin-saturated porous layer of 2 cm thickness. The experimental points are evaluated at a reference temperature equal to the interface temperature. Horizontal and vertical lines indicate possible errors.

the thermal conductivity of the porous medium to the heat capacity per unit volume of the fluid $(\rho c)_f$. The thermal conductivity of the medium κ_m is given by

$$k_m = \epsilon k_f + (1-\epsilon) k_g,$$

where k_g is the thermal conductivity of the glass.

Using the same values of δ (= 0.002), ϵ_T (= 0.7), and $\hat{\alpha}$ (= 0.1) as those used by Sun (1973), our results, for both the critical Raleigh number and the critical wavenumber, agreed very well with Sun's results up to a depth ratio $\hat{d}$ of 0.1. For $\hat{d} = 0.11$, the critical wavenumber calculated by us was almost ten times larger than that calculated by Sun. Further investigation showed that the marginal stability curve was bimodal and, at approximately $\hat{d} = 0.105$, the critical mode shifted from the long-wavelength branch to the short-wavelength branch. Physically, when the depth ratio is small, $\hat{d} \leqslant 0.1$, the instability was dominated by the porous layer. When the depth ratio $\hat{d} > 0.1$, the fluid layer was of sufficient depth to become the more unstable of the two layers, and it became the dominant layer for instability.

The variations of the critical Rayleigh number and wavenumber as functions of the depth ratio are presented in figures 1 and 2. Two theoretical lines are shown: the solid line is for $\delta = 1.77 \times 10^{-3}$, $\epsilon_T = 0.7$, and $\hat{\alpha} = 0.1$, and the dotted line is for $\delta = 3.53 \times 10^{-3}$, $\epsilon_T = 0.4$, and $\hat{\alpha} = 0.1$. The former represents a 4 cm thick porous layer of 3 mm diameter glass beads saturated with water, and the latter represents a 2 cm thick layer of similar beads saturated with 100% glycerin. We note here that we

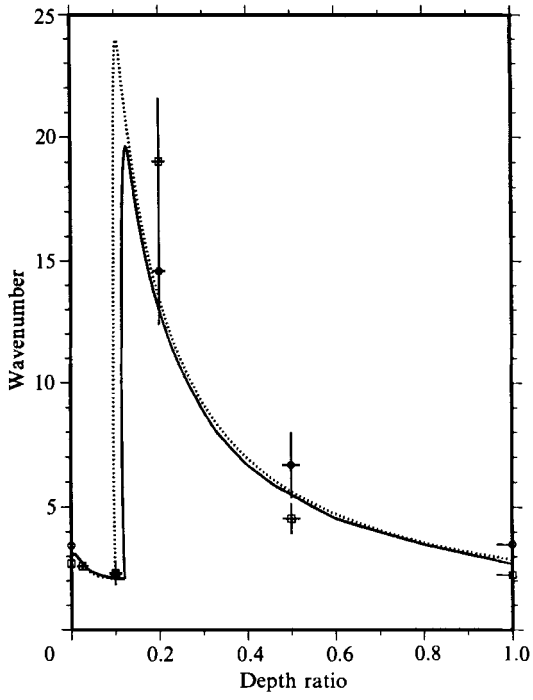

FIGURE 2. Variation of the critical wavenumber with depth ratio. For the parameters used to calculate the solid and the dotted lines, see figure 1. The experimental points are obtained by temperature distributions (squares) and liquid crystal film (circles).

have varied the accommodation coefficient $\hat{\alpha}$ from 0.1 to 4.0 with no noticeable effect on the final result. The Rayleigh number R_m is defined for the porous layer as

$$R_m = \frac{g\alpha \Delta T_m K d_m}{\nu \kappa^*}, \tag{1}$$

in which g is the gravitational constant, α the volumetric expansion coefficient, ΔT_m the temperature difference across the porous layer, K the permeability, d_m the thickness across the porous layer, ν the kinematic viscosity of the saturating fluid, and κ^* the thermal diffusivity of the porous layer defined earlier. The temperature difference across the porous layer can be related to the temperature difference across the combined layer ΔT when the system is in the conduction mode prior to the onset of instabilities,

$$\Delta T_m = \Delta T \left(\frac{\epsilon_T + \hat{d}}{\epsilon_T}\right)^{-1}. \tag{2}$$

In figure 1, we show the rapid decrease of the Rayleigh number R_m with increasing depth ratio $\hat{d}$. The abrupt change in the rate of decrease of the Rayleigh at $\hat{d} \approx 0.13$ is due to the sudden shift of critical condition from the long-wavelength branch to the short-wavelength branch. The sudden increase of the critical wavenumber at the critical depth ratio is shown in figure 2.

Sun (1973) carried out a comprehensive study of convective stability in a two-layer system, including a stability analysis and an experimental investigation. The experiments were conducted in a circular tank 29 cm in diameter and 8 cm in depth.

The solid matrix consisted of glass spheres 6 mm in diameter, and the saturating fluid was water. He found good agreement between the experimentally obtained critical Rayleigh number and the theoretically predicted ones at depth ratios $\hat{d}$ of 0.0609, 0.109, and 0.211. The experimental confirmation of his predictions at $\hat{d} = 0.211$ is in direct conflict with our linear stability results (Chen & Chen 1988) which predict a critical Rayleigh number one-third the value found by Sun and a critical wavenumber approximately ten times as large as that found by Sun. From the experimental data presented in table 5.4 of his thesis (Sun 1973), the critical temperature difference across the tank at $\hat{d} = 0.211$ is approximately 0.5 °C. Such small critical temperature differences could present difficulties in controlling the experiment and obtaining the necessary accuracy for the data. It is important to devise a set of experiments such that (i) the critical temperature difference would be of sufficient magnitude to eliminate such difficulties, and (ii) the convection pattern at the supercritical state can be determined since the heat transfer characteristics at supercritical conditions will be crucially dependent on the convection pattern. Results from this set of experiments can then be used to judge the validity of our linear stability analysis. We have recently carried out such a series of experiments in a rectangular test tank with six different depth ratios ranging from 0 to 1.0. The experimental results were in general agreement with the theoretical predictions, including the drastic change in the critical wavelength between $\hat{d} = 0.10$ and 0.20.

2. Experimental apparatus and procedure

The experiments were performed in the box used by Murray & Chen (1989) to investigate the onset of double-diffusive convection in a porous layer. The box had inside dimensions of 24 cm long × 12 cm wide × 4 cm high. The sidewalls of the box were made of glass, and the top and bottom constant-temperature walls were made of brass. The top wall, which was removable, was provided with passages through which the water from a constant-temperature bath could circulate. The bottom wall was of sandwich construction consisting of an upper plate made of brass and a lower plate made of aluminium, in which water passages were provided. Sandwiched in between these two plates was an RdF Microfoil heat flux sensor with dimensions of 4 cm × 15 cm. This sensor was located at the centre of the aluminium plate, from which sufficient material was removed to accommodate the sensor. In order to ensure good thermal contact between the aluminium plate, the heat flux sensor, and the brass plate, Dow Corning Silicone heatsink compound was embedded in the top and bottom walls near the inside surfaces at the centre and at the periphery of each wall. The box was insulated on all sides and both walls with Styrofoam. Water at different temperatures was supplied by two separate constant-temperature baths. The heat flux sensor was calibrated by filling the box with glycerin and imposing a stable temperature difference using the heat conductivity values given by Segur (1953).

The solid matrix consisted of glass beads with a nominal diameter of 3 mm. The permeability K of such a porous medium was obtained by using the Kozeny–Carmen relation (Combarnous & Bories 1975)

$$K = \frac{d_1^2}{172.8} \frac{\epsilon^3}{(1-\epsilon)^2}, \tag{3}$$

in which d_1 is the diameter of the glass beads and ϵ the porosity. Experiments were performed with six different depth ratios ($\hat{d} = 0$, 0.25, 0.1, 0.2, 0.5, and 1.0): three below and three above the critical depth ratio. These experiments were conducted in

the test tank with a fixed height of 4 cm. The depth of the porous layer d_m must vary according to $d_m = 4/(1+\hat{d})$, which in the present experiments varied from 4 cm to 2 cm. For the $\hat{d} = 0.025$ case, special provision were made to support the top constant-temperature wall 1 mm above the porous layer of 4 cm in depth. When filling the tank with fluid-saturated porous medium, it was important to avoid trapping air bubbles among the glass beads, especially for fluids more viscous than water. We first immersed the glass beads in a beaker which was filled with saturating fluid. Then, the wetted beads were ladled with a spoon into the test tank. When the fluid is very viscous, such as pure glycerin, extra care must be taken since any sudden motion of the spoon would generate a number of air bubbles, which would persist in the fluid for a long time. After the glass beads were packed to the desired height, additional fluid was added to fill the tank to 4 cm in depth. The top constant-temperature plate was then carefully placed on top of the fluid layer, resting on Plexiglas stays placed at the two ends of the tank. Care was taken not to trap any air bubbles between the fluid surface and the top wall.

In order to keep the overall temperature difference across the test tank within reasonable limits so that it is not too small to be determined accurately, and at the same time not too large to incur sizeable property variations, fluids of higher viscosity were used as the depth ratio was increased. Four different fluids were used: water for $\hat{d} = 0$, 0.025, and 0.1; 60% glycerin–water solution for $\hat{d} = 0.2$; 90% glycerin–water solution for $\hat{d} = 0.5$; and 100% glycerin for $\hat{d} = 1.0$. For these fluids, the diffusivity ratio ϵ_T varied from 0.4 (glycerin) to 0.7 (water).

The size of the convection cells was determined by three different methods. In the first method, it was inferred from the temperature distributions measured both in the longitudinal and transverse directions. Temperatures at selected locations at a horizontal plane 2 cm above the bottom of the tank were measured by thermocouples which were fixed onto a grid. The grid was made of a Plexiglas frame spanning the inside of the box with two slightly stretched nylon lines, one of the longitudinal direction and the other in the transverse direction. Thermocouples made of 36-gauge copper and constantan wires were attached onto the nylon wires; 14 of these were in the longitudinal direction and 6 were in the transverse direction. The distances between the thermocouples were adjustable to accommodate the disparate wavelengths anticipated from the stability analysis. The thermocouple output was converted into temperatures by a Fluke Datalogger.

For experiments with $\hat{d} \geqslant 0.2$ in which the fluids were glycerin–water solutions, convection patterns in the fluid layer at supercritical states may be detected by shadowgraphs. This is because the rate of change of the index of refraction with respect to temperature for glycerin is approximately three times as large as that for water. At 15 °C, the respective values are 2.25×10^{-4} °C^{-1} (Segur 1953) and 0.7×10^{-4} °C^{-1} (Weast 1975). In these cases, the wavelengths obtained from temperature measurements were compared with those obtained by shadowgraph.

The third method involved the use of a liquid crystal film. It became evident from the temperature readings early in our investigation that the convection pattern was three-dimensional. In order to visualize the pattern over the entire tank, we chose the technique using a liquid crystal film. The film was glued to a Plexiglas sheet 1.58 cm ($\frac{1}{16}$ in.) thick, which was of the same size as the top cooling plate. The temperature range of the film was from 25 °C (orange in colour) to 30 °C (blue in colour). Intermediate temperatures appeared in shades of yellow and green. At the desired condition when the convection cells were fully developed, the cooling plate was removed, and the sheet with the liquid crystal film was carefully placed on top of the

fluid layer so as not to trap any air bubbles under the sheet. With practice, the entire operation could be completed in less than two minutes. The colour pattern in the liquid crystal film would slowly emerge, and it was recorded by a camera mounted vertically above the tank.

Each experiment was started by increasing the temperature of the bottom wall by a predetermined amount and, at the same time, decreasing the temperature of the top wall by the same amount. In this manner, the mean temperature was maintained close to room temperature. The diffusion time based on a 2 cm layer of 100 % glycerin was 2200 s. The temperature difference across the tank was adjusted every 2 hours. The voltage output of the heat flux meter and temperatures at selected points were recorded every minute; these readings indicated that the equilibrium was generally established within 40 minutes. The temperature difference across the tank was slowly increased to approximately 20 °C in five or six steps. The same experiment with the same packing of glass beads was repeated a number of times so that there would be a good coverage of data points within the temperature difference range. A total of 39 experiments were performed.

3. Experimental results

3.1. *Critical Rayleigh number*

For data evaluation, the porosity of the porous medium must be measured *in situ*. This is particularly important for this set of experiments because the glass beads must be packed carefully in order to present a nearly flat interface. A photo showing the experimental set-up for $\hat{d} = 1.0$ is presented in figure 3. It can be seen that the glass beads are packed in a number of horizontal rows with hardly any defect. The measured values of porosity ϵ obtained by slowly filling four different packings of the glass beads with water ranged from 0.341 to 0.350, with an average of 0.345, which was taken as the porosity of the medium. It is noted there that a random packing of glass beads usually yields an ϵ of 0.390. Both values are well within the theoretical range of 0.259 to 0.875 given by Scheidegger (1974).

To check the experimental system, we ran a set of experiments for $\hat{d} = 0$, a 4 cm thick layer of water-saturated glass beads. The heat flux curve is shown in figure 4, with a critical ΔT of 15.2 °C. The physical properties are evaluated at the mean temperature of 24 °C using the correlation given by Burretta (1972) for water. The critical Rayleigh number is found to be 40.07, as shown in figure 5, which is in excellent agreement with the theoretical value of $4\pi^2$ given by Lapwood (1948) and the experimental results of Combarnous & LeFur (1969), Elder (1967), Katto & Masuoka (1967), and Burretta (1972).

The same procedure was followed to determine the critical ΔT for $\hat{d} = 0.025$ to 1.0. When converting these critical ΔT to Rayleigh numbers, a question arises as to what temperature to use for the evaluation of the physical properties. Since the dominating convection occurs in the porous layer at small $\hat{d}$ and in the fluid layer at large $\hat{d}$, we calculated the Rayleigh numbers based on the physical properties at three different temperatures: T_{mp}, the mean temperature of the porous layer; T_{mf}, the mean temperature of the fluid layer; and T_0, the temperature at the interface. These Rayleigh numbers, together with the theoretical value predicted by the linear stability theory, are shown in table 1. It can be seen that the Rayleigh numbers evaluated at T_0, the interface temperature, give the least relative error with respect to the predicted value. This set of critical Rayleigh numbers is shown in figure 1 in comparison with the theoretical curve. The agreement is quite good. Error bars are

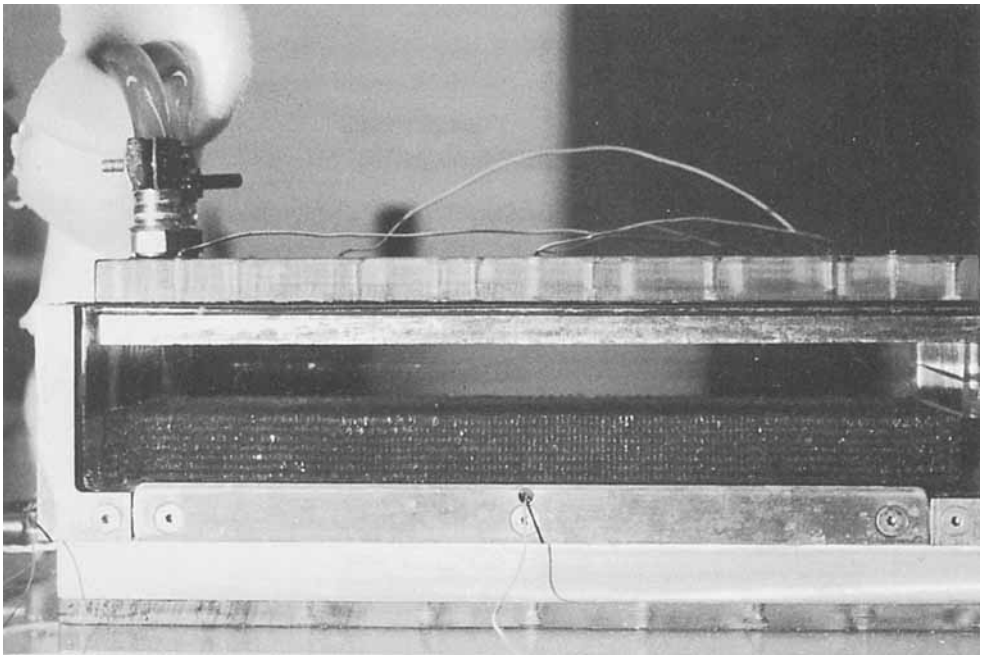

FIGURE 3. Experimental set-up for $\hat{d} = 1.0$ case with 100% glycerin. The glass beads are packed carefully in regular horizontal rows to obtain a smooth, flat interface.

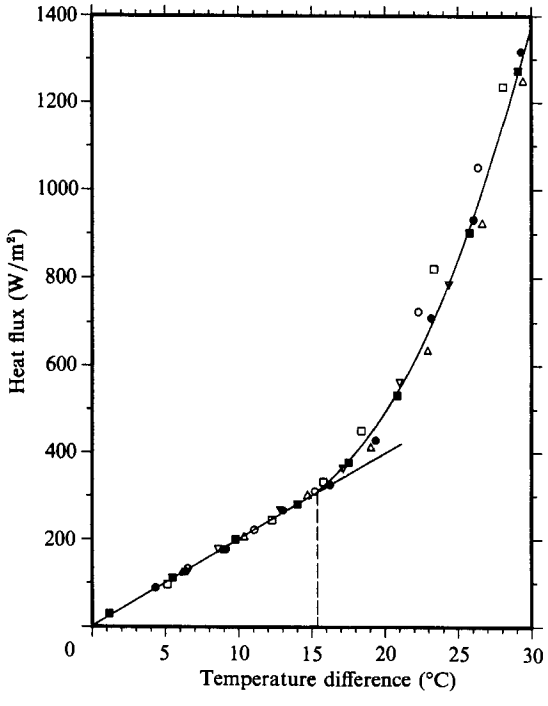

FIGURE 4. Experimental heat flux curve for a 4 cm thick porous layer. Different symbols denote different sets of experiments with the same packing of glass beads.

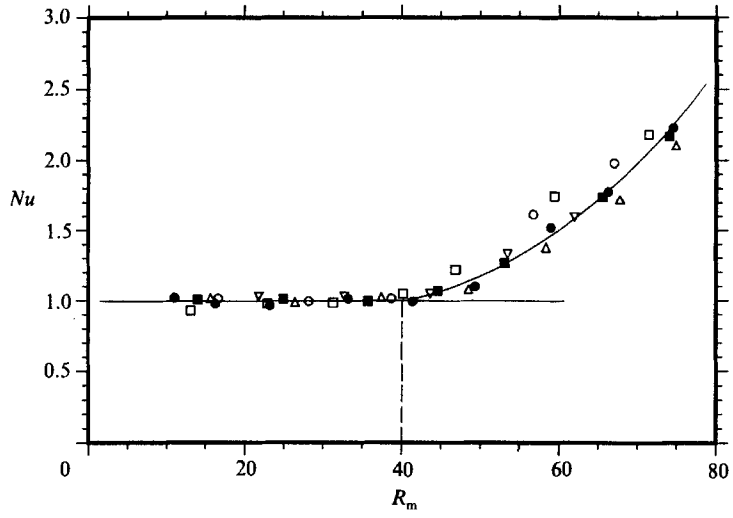

FIGURE 5. Nusselt-number results for the porous layer.

			$R_{m,exp}$ (T_{ref} °C)			
$\hat{d}$	d_m (cm)	ΔT_{crit} (°C)	T_{mp}	T_0	T_{mf}	$R_{m,Th}$
0	4.0	15.2	40.07 (24)	—	—	39.46
0.025	4.0	13.8	36.80 (25)	31.82 (18)	31.82 (18)	33.22
0.1	3.64	12.8	25.40 (23)	17.57 (18)	17.57 (18)	21.26
0.2	3.33	11.6	4.71 (26)	3.95 (22)	3.65 (20)	2.71
0.15	2.67	12.8	0.190 (27.5)	0.159 (25)	0.110 (20)	0.120
1.0	2.00	11.7	0.0145 (28)	0.0124 (26)	0.0093 (22.5)	0.0139

TABLE 1. Experimental values for the critical Rayleigh number

Fluid	$\hat{d}$	T_{ref} °C	$\rho \times 10^3$ kg/m³	$C_p \times 10$ 10 J/kg °C	$\nu \times 10^{-6}$ m²/s	$\alpha \times 10^{-4}$ °C⁻¹	k_f W/m °C	$\kappa_f \times 10^{-6}$ m²/s	$k^* \times 10^{-6}$ m²/s	ϵ_T
Water	0	24	0.997	4.16	0.919	2.48	0.602	0.145	0.201	0.720
Water	0.025, 0.1	18	0.999	4.17	1.06	1.85	0.594	0.143	0.200	0.713
60% Glycerin	0.2	22	1.155	3.10	8.60	5.45	0.379	0.106	0.212	0.50
90% Glycerin	0.5	25	1.236	2.559	125.4	6.15	0.300	0.094	0.229	0.410
100% Glycerin	1.0	26	1.262	2.41	673.5	6.10	0.284	0.093	0.239	0.389

TABLE 2. Summary of fluid properties

shown for each data point. The horizontal bar indicates the possible error resulting from the uncertainties in the measurement of the depth of the two layers. The vertical bar indicates the uncertainties in the Rayleigh-number determination. The major source is due to the uncertainty of the critical temperature difference. The physical properties of the fluid evaluated at T_0 are summarized in table 2.

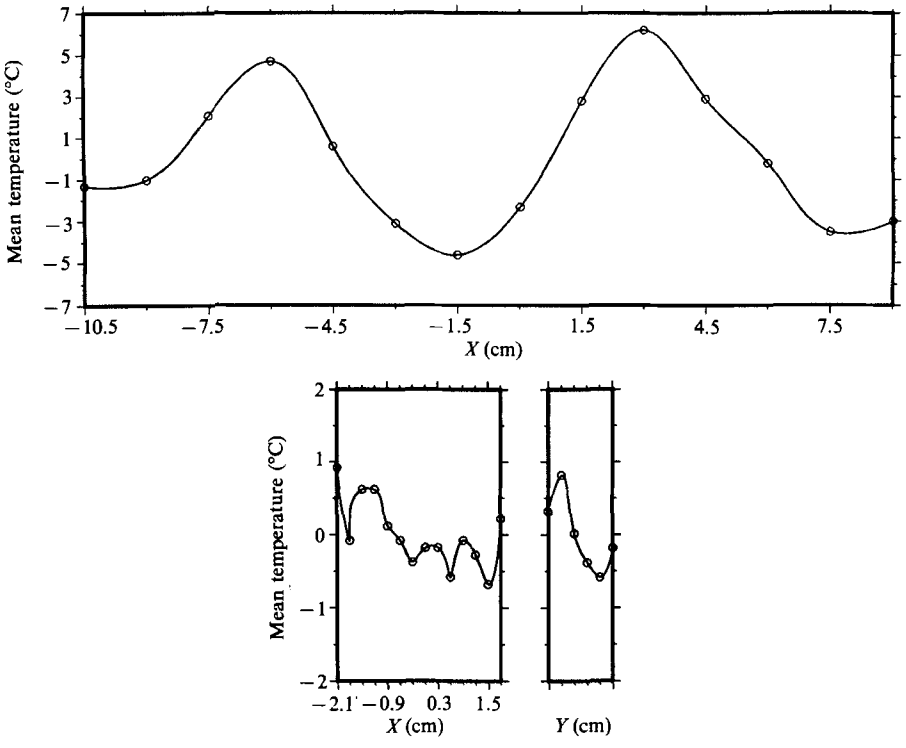

FIGURE 6. Temperature distributions in the porous layer: x denotes the longitudinal direction and y denotes the lateral direction. (*a*) $\hat{d} = 0.1$ at $\Delta T = 21.2\,°\text{C} = 1.54\Delta T_{\text{crit}}$; (*b*) $\hat{d} = 0.2$ at $\Delta T = 33.5\,°\text{C} = 2.89\Delta T_{\text{crit}}$.

3.2. *Critical wavelength*

Temperature distributions in the longitudinal directions for the cases of $\hat{d} = 0.1$ at $\Delta T = 21.2\,°C$ and $\hat{d} = 0.2$ at $\Delta T = 33.5\,°\text{C}$ are shown in figures 6(*a*) and 6(*b*). The temperature distribution in the lateral direction for $\hat{d} = 0.2$ is also shown in figure 6(*b*). It should be noted that these two graphs have the same lengthscale to emphasize the abrupt decrease in the critical wavelength. An upward motion of the fluid would induce a relatively higher temperature reading, whereas a downward motion of the fluid would induce a relatively lower temperature. For $\hat{d} = 0.1$, the wavelength of the convection cells obtained by measuring the distance either between the maxima or the minima of the longitudinal temperature distribution was 9 cm. For $\hat{d} = 0.2$, there were four minima and three maxima, and the average wavelength obtained was 1.1 cm, an eightfold decrease for a slight increase in the fluid layer thickness. We have shown the temperature distributions at supercritical states so that the structure of the convection cells is clearly discernible. These fully developed cells could be traced to those starting cells at temperature differences slightly larger than the critical value, and the wavelengths of these cells were approximately equal.

The temperature distribution in the lateral direction for $\hat{d} = 0.2$ indicated that the convection pattern was three-dimensional. This was true for every depth ratio except 0. In some cases at $\hat{d} = 0$ the convection pattern was two-dimensional, as shown in flow visualization pictures made by Murray (1986). However, there were instances in which the pattern was three-dimensional. For $\hat{d} > 0$, the convection pattern was invariably three-dimensional. For $\hat{d} = 0.2$, the fluid used was a 60% glycerin–water

$\hat{d}$	Theory	Temperature distribution	Liquid crystal	Shadowgraph
0 (2)	8.0	9.25 (5)	7.3 (6)	—
0.025 (50)	9.56	9.65 (5)	—	—
0.1 (14)	10.60	9.9 (5)	11.0 (20)	—
0.2 (7)	1.75	1.1 (14)	1.58 (15)	1.34 (25)
0.5 (4)	3.03	3.7 (14)	3.13 (20)	3.38 (20)
1.0 (4)	4.46	5.58 (9)	4.79 (18)	4.64 (17)

TABLE 3. Experimental values of the critical wavelength (cm) with estimated percentage errors (given in parentheses)

solution, and we were able to obtain shadowgraphs, with faint shadows showing a few of the convection cells at $\Delta T = 35.5$ °C. The wavelength was estimated to be 1.5 cm, as compared to the value of 1.1 cm obtained from the temperature distribution. Wavelengths of convection cells at $\hat{d} = 0.5$ and 1.0 were similarly determined from the temperature distributions obtained from the experiment.

The convection patterns as revealed by the liquid crystal film are shown in figures 7, 8 and 9 (plates 1, 2, and 3). In figure 7, patterns for $\hat{d} = 0$ and 0.1 are shown. The temperature differences across the tank just prior to these photos being taken are given in the figure caption; they range between 1.5 and 3.0 times the critical temperature difference. For $\hat{d} = 0$, there were three prominent upward plumes showing in blue. The downward plumes in orange were distributed around the edge of each cell. At $\hat{d} = 0.1$, the convection cell was noticeably larger than in the previous case. When the depth ratio was increased to 0.2, figure 8, the convection cells became much smaller and they were distributed more or less evenly in the central portion of the tank. As $\hat{d}$ was further increased, the convection cell became larger since the convection motion was essentially confined within the upper fluid layer. For $\hat{d} = 0.5$ (figure 8), the cells were regularly spaced in the tank. For both $\hat{d} = 0.2$ and 0.5, the temperature differences between the hot and cold plumes were less than 5 °C, resulting in a colour range from yellow to blue. For $\hat{d} = 1.0$, we present in figure 9 a liquid crystal pattern and a shadowgraph, taken at approximately the same time. The convection cells continued to increase in size. It can be seen that the shadowgraph shows overlapping cellular structure since the light path traversed through the entire width of the tank.

Estimates of wavelengths from these flow patterns are listed and compared to those predicted by theory and obtained by other measurement techniques in table 3 and the data points shown in figure 2. Even though the linear stability analysis was done for a two-dimensional flow pattern, there is some degree of agreement between the theoretical and the experimental values.

4. Conclusions

(*a*) The precipitous decrease of the critical Rayleigh number R_m as the thickness of the overlying fluid layer increases from zero as predicted by the linear stability theory was confirmed by experimental results.

(*b*) The sudden decrease in the critical wavelength between $\hat{d} = 0.1$ and 0.2 as predicted by the linear theory was confirmed by temperature measurements and by the pattern exhibited in the liquid crystal film.

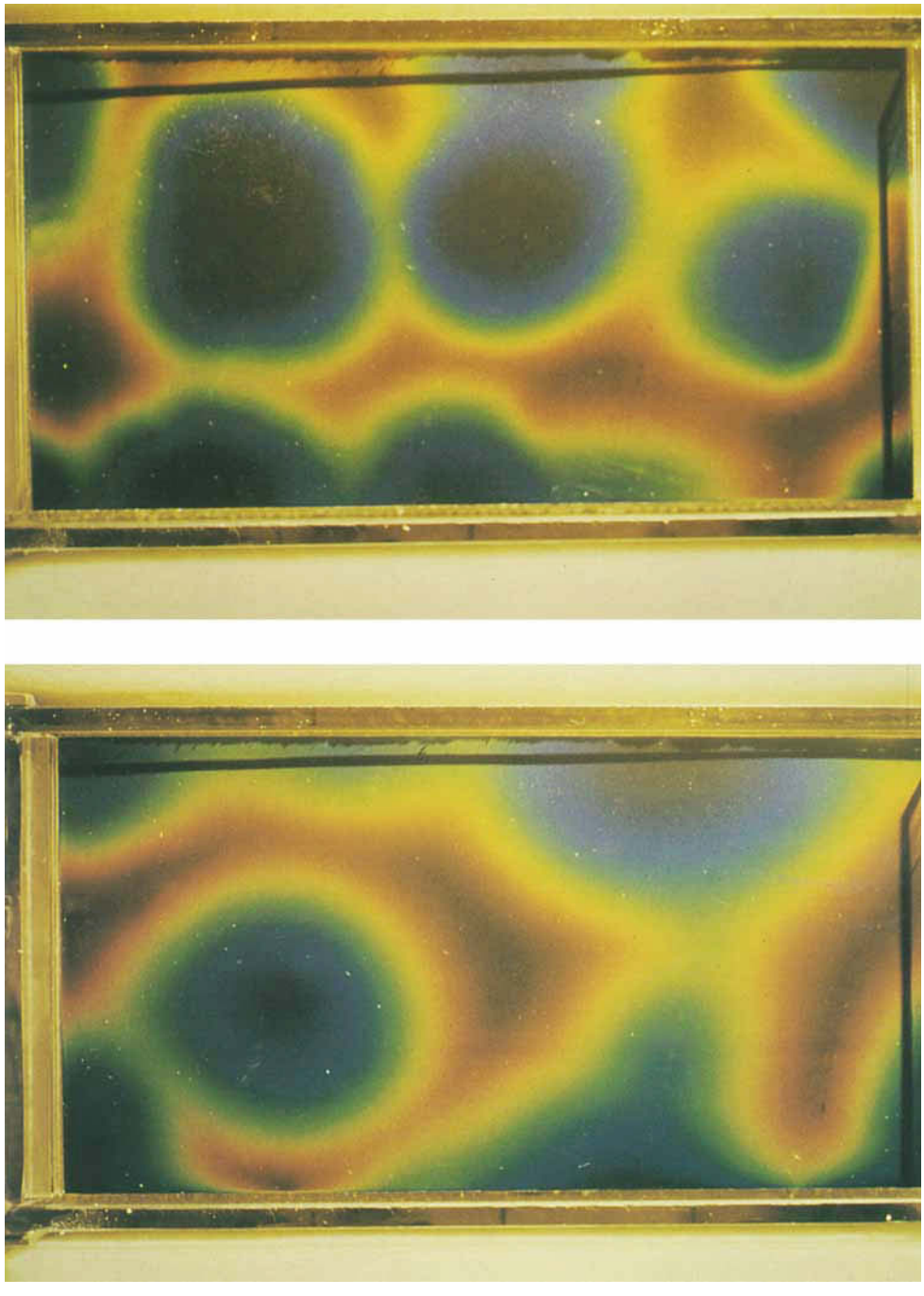

FIGURE 7. Liquid crystal film fixed to a transparent wall showing convection patterns for $\hat{d}=0$ (top) and $\hat{d}=0.1$ (bottom). Blue signifies 30°C and orange 25°C. The convection cells are three-dimensional, and they increase in size from $\hat{d}=0$ to 0.1. The picture was taken at 1.46 ΔT_{crit} for $\hat{d}=0$ and 1.59 ΔT_{crit} for $\hat{d}=0.1$.

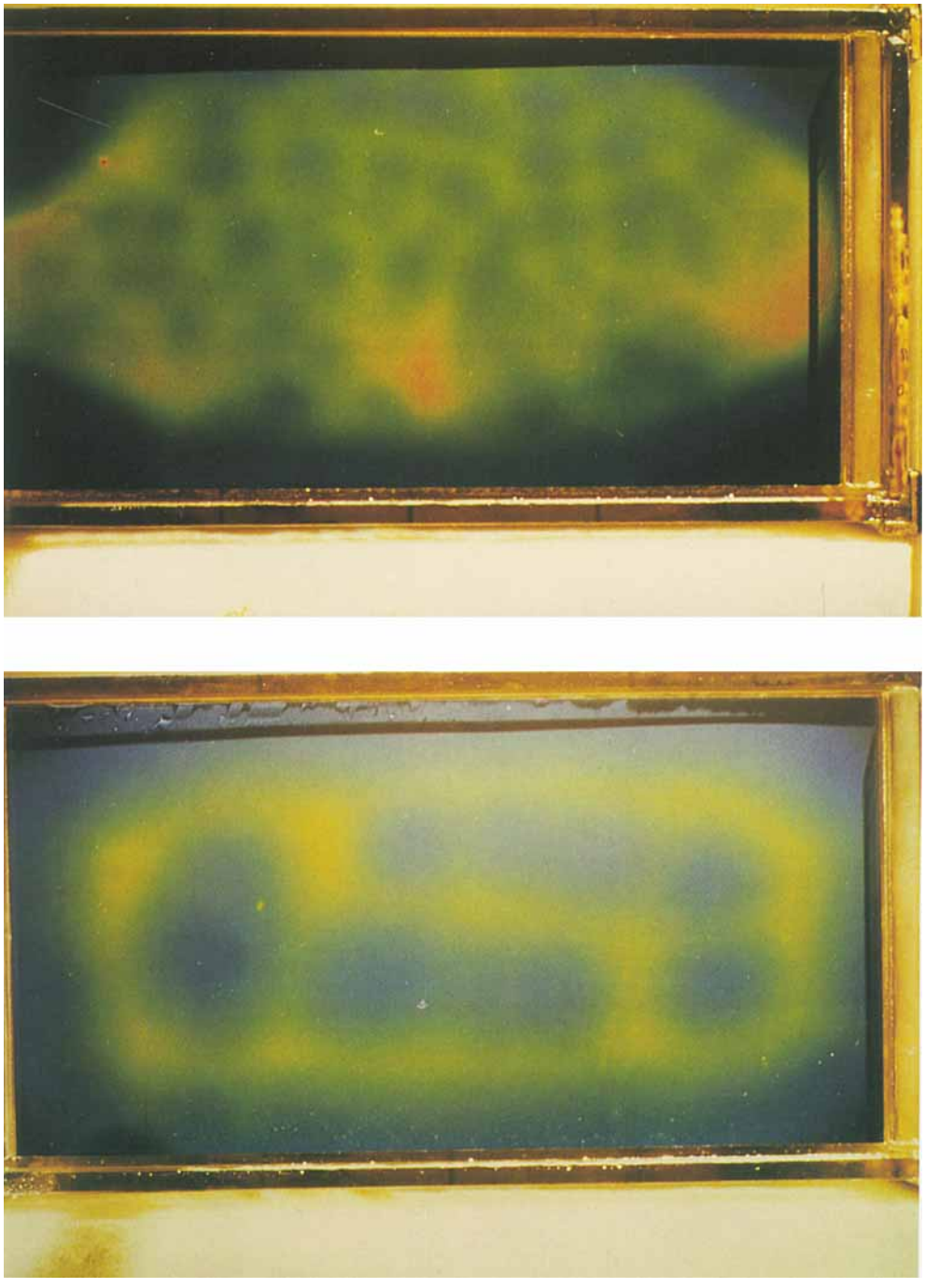

FIGURE 8. Convection patterns for $\hat{d}$=0.2 (top) at 3.0 ΔT_{crit} and $\hat{d}$=0.5 (bottom) at 1.33 ΔT_{crit}. Note the dramatic decrease in the wavelength from $\hat{d}$=0.1 (figure 7) to $\hat{d}$=0.2.

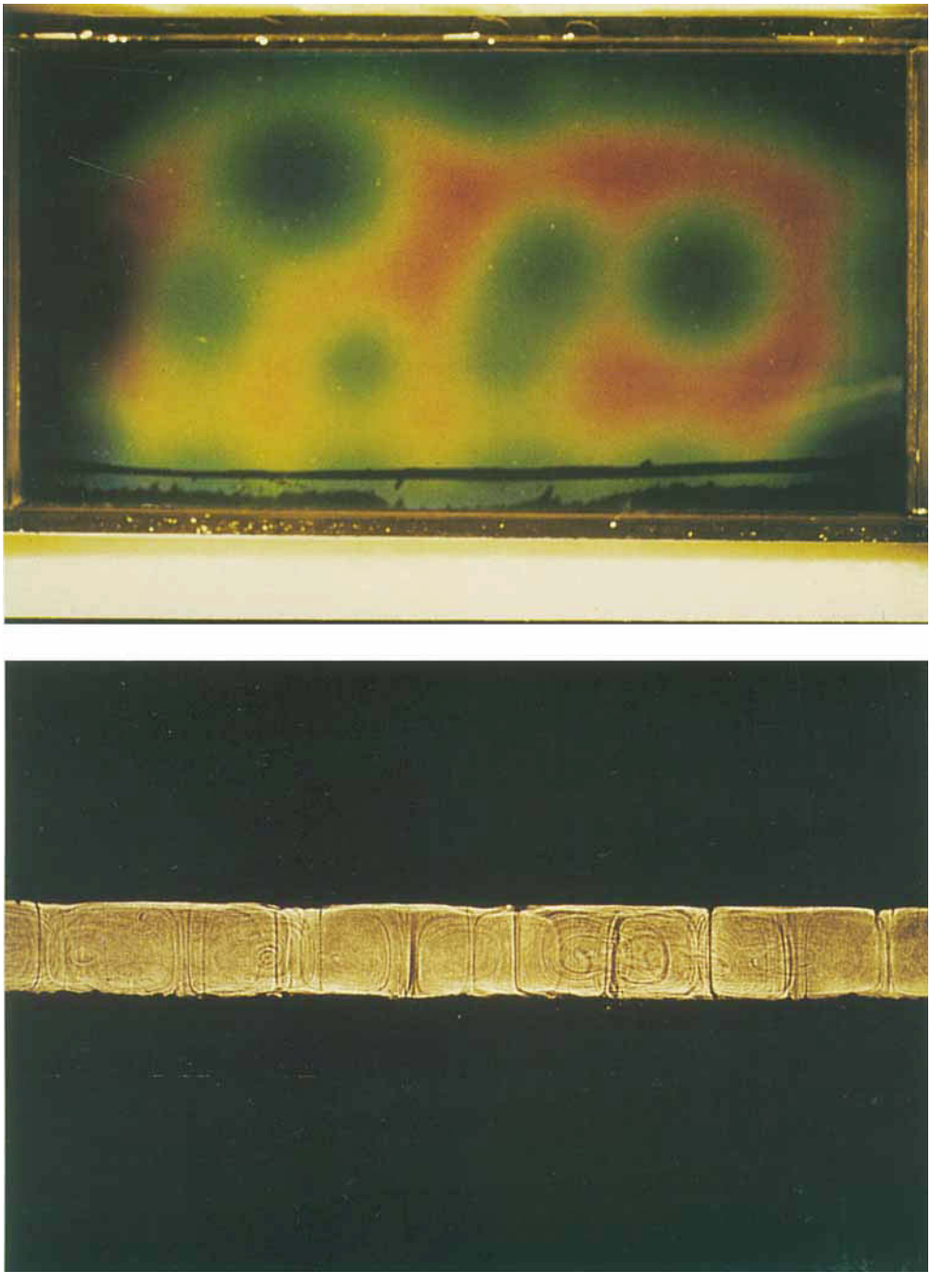

FIGURE 9. Convection pattern (top) for $\hat{d}$=1.0 at 1.98 ΔT_{crit} and shadowgraph (bottom) taken at approximately the same time. Since the shadowgraph integrates the flow structure through the entire width of the tank, one can discern the three-dimensional effect.

(*c*) It was found that the convection cells were generally three-dimensional.

The financial support of NASA through Grant NAG 3-723 and of NSF through Grant MSM-8702732 is gratefully acknowledged.

REFERENCES

BEAVERS, G. S. & JOSEPH, D. D. 1967 Boundary conditions at a naturally permeable wall. *J. Fluid Mech.* **30**, 197–207.

BURRETTA, R. J. 1972 Thermal convection in a fluid filled porous layer with uniform internal heat sources. Ph.D. dissertation, University of Minnesota, Minneapolis.

CHEN, F. & CHEN, C. F. 1988 Onset of finger convection in a horizontal porous layer underlying a fluid layer. *Trans. ASME* C: *J. Heat Transfer* **110**, 403–409.

COMBARNOUS, M. A. & BORIES, S. A. 1975 Hydrothermal convection in saturated porous media. *Adv. Hydrosci.* **10**, 231–307.

COMBARNOUS, M. A. & LEFUR, B. 1969 Transfert de chaleur par convection naturelle dans une conche poreuse horizontale. *C. R. Acad. Sci. Paris* B **269**, 1009–1012.

ELDER, J. W. 1967 Steady free convection in a porous medium heated from below. *J. Fluid Mech.* **27**, 29–48.

KATTO, Y. & MASUOKA, T. 1967 Criterion for onset of convection flow in a fluid in a porous medium. *Intl J. Heat Mass Transfer* **10**, 297–309.

LAPWOOD, E. R. 1948 Convection of fluid in a porous medium. *Proc. Camb. Phil. Soc.* **44**, 508–521.

MURRAY, B. T. 1986 Experimental and numerical investigation of double-diffusive convection in a horizontal layer of porous medium. Ph.D. dissertation, University of Arizona, Tucson.

MURRAY, B. T. & CHEN, C. F. 1989 Double-diffusive convection in a porous medium. *J. Fluid Mech.* **201**, 147–166.

SCHEIDEGGER, A. E. 1974 *The Physics of Flow Through Porous Media*, 3rd edn., p. 21. University of Toronto Press.

SEGUR, J. B. 1953 Physical properties of glycerol and its solutions. In *Glycerol* (ed C. S. Miner & N. N. Dalton), pp. 238–334. Reinhold.

SUN, W. J. 1973 Convective instability in superposed porous and free layers. Ph.D. dissertation, University of Minnesota, Minneapolis.

WEAST, R. C. 1975 (Ed.) *Handbook of Chemistry and Physics*. CRC Press.